A refined reverse Monte Carlo analysis of the structure of vitreous P_2O_5

2000 J. Phys.: Condens. Matter 12 8809

(http://iopscience.iop.org/0953-8984/12/41/306)

J. Phys.: Condens. Matter **12** (2000) 8809–8818. Printed in the UK PII: S0953-8984(00)12854-1

A refined reverse Monte Carlo analysis of the structure of vitreous P_2O_5

U Hoppe

Department of Physics, Rostock University, Rostock D-18051, Germany

Received 28 March 2000, in final form 29 August 2000

Abstract. The improved reverse Monte Carlo simulations of the structure of vitreous P_2O_5 are constrained by neutron and x-ray scattering data both covering large ranges of momentum transfer, and by geometric constraints which are different for the terminal and bridging oxygen sites. The analysis of the model structures reveals the anisotropy of the threefold-linked PO_4 tetrahedra with different P–O bonds and O–O edges of the terminal and bridging oxygen sites. The O–P–O and P–O–P bond angles possess mean values of 109 and 139°. Flattened network cages formed of the P atoms and the bridging O sites are identified in the models. Their formation is enhanced by the more real geometry of the PO_4 units. The first peak of the x-ray and neutron diffraction data is related to the lateral dimension of the cages of about 0.47 nm.

1. Introduction

The structure of the unusual glass of phosphorus pentoxide was studied by neutron [1] and x-ray (Ag Kα) [2] diffraction. The numbers of first neighbours determined from the experiments agree with the facts of a continuous random network formed of threefold corner-linked PO_4 tetrahedra. The linking of the PO_4 units which is illustrated in figure 1 of [1] was concluded from Raman spectroscopy [3] and ^{31}P magic angle spinning NMR [4]. Since the P–P peak interferes with other second-neighbour distances the P–P coordination number is extracted from the diffraction data only roughly [2]. Information about the medium-range order (MRO) of the glass is found in the range of the first diffraction peaks [5, 6]. Different from the single-component glasses of silica and germania with a single first peak [7, 8] x-ray scattering of vitreous (v-) P_2O_5 yields a double peak with maxima at $Q = 13$ nm^{-1} and 20 nm^{-1} [9]. Q is the magnitude of the scattering vector with $Q = 4\pi/\lambda \sin\theta$ with λ the radiation wavelength and 2θ the scattering angle. Both features of the first peak were attributed to a layer-like structure with different characteristic lengths, D with $D = 2\pi/Q$, along the layers (0.31 nm) and perpendicular to them (0.47 nm) [9]. A flattened variant of the corrugated sheets known of the structure of crystalline P_2O_5 form III [10] was suggested for the glass structure. Other authors [11] prefer a relation of the glass structure to that of the P_4O_{10} crystal (form I) [12]. Better than simple comparisons with the structures of the crystals, reverse Monte Carlo (RMC) simulations [13] provide a tool to examine the relations between diffraction data and structural features. Our first RMC work on v-P_2O_5 [2] reproduces the double maximum of the x-ray data. The first peak component at 13 nm^{-1} was attributed to P–P second-neighbour distances according to binary systems of atoms and voids such as suggested for amorphous Ge [14] and SiO_2 or GeO_2 [5]. The second peak component was related to the environment of the one

0953-8984/00/418809+10$30.00

terminal oxygen atom of the PO_4 unit [2], which has no analogy in the structures of v-SiO_2 or v-GeO_2.

In our first RMC runs [2] the constraints used for the two oxygen sites did not differ though the split distance peak of P–O bonds in the real-space correlation function, $T(r)$, [1] evidences different bond lengths to the terminal (O_T) and the bridging (O_B) oxygen atoms. Also due to the use of limited Q-ranges of the $S(Q)$-data clear relations of the O_Ts and O_Bs to both fractions of the P–O distances were not reproduced. Only after the RMC runs have the O_T and O_B sites of a final model been differentiated to study their effects in the MRO [2]. Further RMC work was started with differentiations of the O_Ts and O_Bs from the very beginning of the simulations. Different lengths of the P–O_T and P–O_B bonds and of the O_T–O_B and O_B–O_B tetrahedral edges are controlled by additional constraints. First results have been published preliminarily [15]. Here the RMC runs are repeated again using larger Q-ranges of the neutron and x-ray structure factors. X-ray data covering a Q-range up to 310 nm^{-1} obtained by synchrotron experiments with high-energy photons are available [16]. With these data a smaller width of the peak of the P–P distances was found than before [2]. The present work reports the analysis of the new RMC models, i.e. the partial correlations, the bond angle distributions and features of the MRO of the final models.

2. Modelling

The RMC code here applied differs from that of McGreevy and Pusztai [13] only in the handling of the coordination constraints. Here only maximum numbers, N_{ij}, are defined and the instantaneous N_{ij} do not affect the calculation of χ^2. The criterion for the successive change of the configurations of 1400 atoms in the cubic model boxes with edge lengths of 2.7 nm chosen according to the density of v-P_2O_5 and with periodic boundary conditions is to improve the agreement between the experimental and the model structure factors, $S_k(Q)$. Thus, the procedure is a fit of the experimental $S_k(Q)$-data using a Monte Carlo approach with a minimization of χ^2 where

$$\chi^2 = \sum_{k,l} [S_{k,\mathrm{exp}}(Q_l) - S_{k,\mathrm{mod}}(Q_l)]^2. \tag{1}$$

k stands for X and N, i.e. the x-ray and neutron data, and l for the measuring points. The new position of an arbitrarily chosen atom is accepted in the case of $\chi^2_m < \chi^2_{m-1}$ where $m-1$ denotes the move accepted just before. Different from simple relaxations, the probability $p = \exp[-(\chi^2_m - \chi^2_0)/s]$ determines which of the unfavourable moves is accepted, as well. The value s has a similar meaning to a temperature factor.

The starting configuration of the present work was a final RMC model of our first simulations of v-P_2O_5 [2] where most PO_4 units already possess one terminal P–O bond. P sites of higher coordination than four and fourfold linked PO_4 units were suppressed [2]. Since the models have a few defects such as some PO_3 units and two terminal bonds in other PO_4 units some further modifications were made. In case of the few PO_3 units having no terminal P–O bonds an oxygen atom was added as an O_T and removed from a PO_4 unit with two terminal P–O bonds. Thus, each P site was coordinated with one O_T, which is also the case for the final RMC models. For the few defective P–O_B bonds not bridging a second P site, from time to time, the O_B site was exchanged with the O_T of the same PO_4 unit. After several thousands of moves, finally, the models were relaxed by impeding the rupture of the P–O bonds. In this process the topology of the older RMC models [2] is changed only partially.

In our first RMC work of the structure of v-P_2O_5 [2] the $S_X(Q)$ and $S_N(Q)$ data were used up to Q_{max} of 200 and 250 nm^{-1}, which was too small to resolve the two peaks of P–O

distances. In the new RMC simulations the $S_X(Q)$ [16] and $S_N(Q)$ [1] data are fitted with Q_{max} of 310 and 470 nm^{-1}. In our first work [2] the O_Ts and O_Bs were differentiated only after the RMC runs to discuss their different contributions to the MRO. The P–O bond lengths were not equivalent to the two P–O peaks observed [1]. Hence, the P–O_B–P angles of the models are affected by undue P–O_B distances. The first-neighbour P–O and O–O peaks of the neutron correlation functions, $T(r)$ [1], make it meaningful to differentiate the P–O_T and P–O_B bonds and the O_T–O_B and O_B–O_B tetrahedral edges (cf also the crystalline forms of P_2O_5 [10, 12, 17]). Therefore, the O_Ts and O_Bs are treated as different atomic species. Accordingly, they are allowed to form one or two P–O bonds, respectively. Each P atom can attach one O_T and three O_B neighbours. Edge-connected PO_4 units are suppressed.

Minimum separation distances of 130, 218 and 270 pm were chosen for the P–O, O–O and P–P distances [2]. Commonly, the distance distributions of the first-neighbour peaks are constrained by the high-Q oscillations of the $S(Q)$-data. Thus, they should not be affected by the minimum separation distances, whose aim is only to suppress unreasonably short pair distances [13]. Since scattering cannot differentiate the O_Ts and O_Bs, e.g. by changing the contrast, this principle is partially ignored in the present RMC fits. The different distances of both O species are controlled by additional separation constraints. Otherwise, different P–O bonds and O–O tetrahedral edges are not obtained. A larger minimum separation distance of 150 pm is introduced for the longer P–O_B bonds. This value lies in the middle between the lengths of 143.2 and 158.1 pm obtained for the P–O_T and P–O_B bonds, whose peaks are well resolved in the $T(r)$ function [1]. The differentiation of the tetrahedral edges is difficult where with a mean of 244 pm the O_B–O_B edges are shorter than the O_T–O_B edges at 257 pm [1]. Their peaks are not fully resolved in the $T(r)$-data. Therefore, not the middle value but a shorter one at 246 pm is taken for the new separation distance of the longer O_T–O_B edges. A distance of 250 pm would be a rather strong choice. Since in a PO_4 unit only one O_T exists O_T–O_T edges cannot occur. Thus, the minimum separation distance for O_T–O_T pairs is chosen as 282 pm to exclude contributions to the O–O peak at 0.25 nm. On the other hand, a distance of 282 pm is shorter than that of nearest neighbours of O atoms which do not belong to the same PO_4 unit, cf also the crystal structures [10, 12, 17].

3. Results

The final $S(Q)$-functions of the RMC models well agree with the experimental $S_N(Q)$- [1] and $S_X(Q)$- [16] data in the full Q-range (cf figure 1). The pair distributions, $g_{ij}(r)$, averaged from six model configurations are shown in figure 2. As intended, the P–O_B bond and the O_T–O_B tetrahedral edges are longer than the P–O_T and O_B–O_B distances, respectively. The lengths of the O_B–O_B edges, however, form two unreasonable spikes on both sides of the expected peak. All mean first-neighbour distances are little larger than those obtained by fitting the peaks with symmetric Gaussian functions [2], which must be due to the asymmetry of the distance distributions obtained from the RMC models. An imperfection of the configurations is the absence of a second P neighbour for 5% of the O_B atoms. Obviously, a few links of the model networks are not reasonably chosen. Some stress arising from such links causes significant spikes in the O_B–O_B and O_T–O_T correlations at their minimum separations of 218 and 282 pm, respectively. Further improvement of the models would require more computing time or may exceed the capabilities of RMC. Since the agreement of the $S(Q)$-data shown in figure 1 is already excellent there is no gradient of the χ^2-parameter left which would force the few dangling P–O_B bonds to bridge a second P neighbour. We remember the uncertainty of the experimental $S(Q)$-data themselves: the fit of the P–O peak [1, 2] resulted in numbers

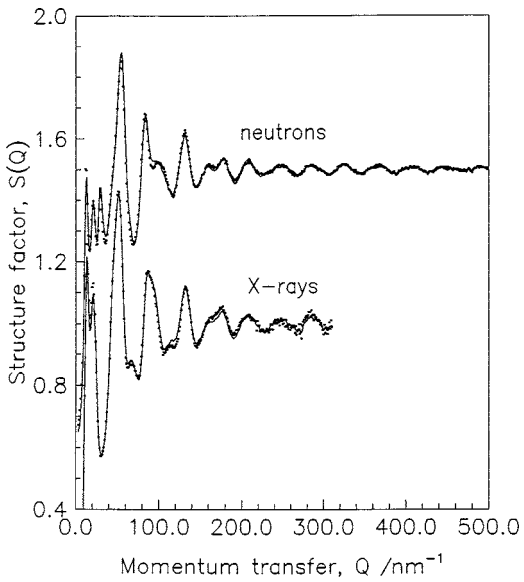

Figure 1. Comparison of the experimental neutron [1] and x-ray [16] structure factors (dots) with those calculated from the final RMC models (lines). The upper functions are shifted by 0.5 for clarity of the plot.

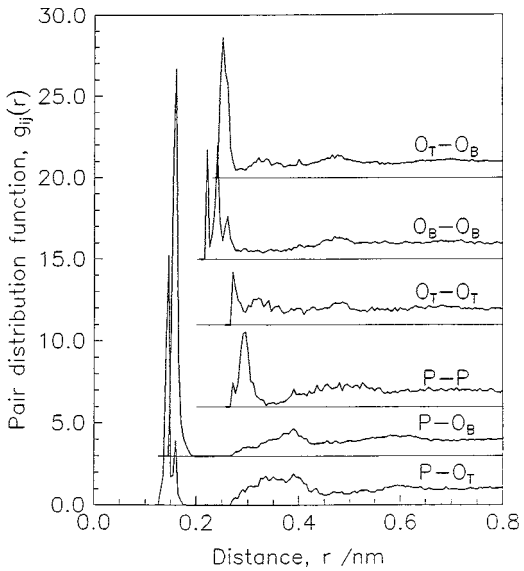

Figure 2. Pair distribution functions, $g_{ij}(r)$, of vitreous P_2O_5 obtained from six RMC configurations. In the simulations the O_T and O_B sites have been treated as species with different minimum separation and coordination constraints.

N_{PO} of 3.9 instead of four. An RMC fit cannot improve the information of the experimental data, which are affected by subtle systematic errors and some noise.

The O–P–O angles of six RMC configurations have been averaged. Not only the small fraction of PO_3 units (5%) which is due to imperfect O_B sites of the models is excluded from

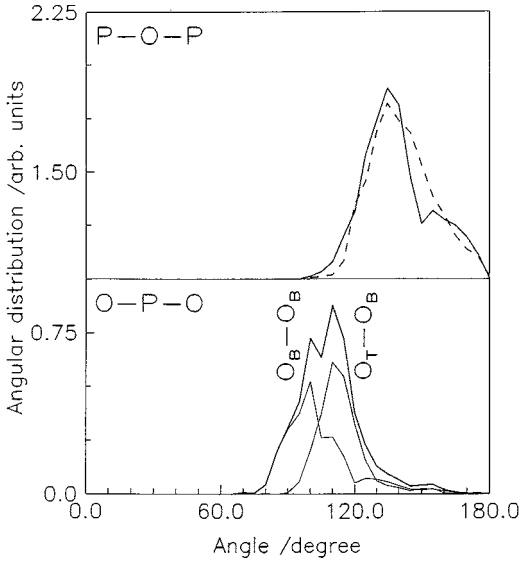

Figure 3. Angular distributions of the P–O–P bridging and the O–P–O intratetrahedral angles of v-P_2O_5 averaged from six RMC configurations. The dashed-lined function is a result of earlier RMC work [2]. The distribution of O–P–O angles is separated into the fractions of the O_B–P–O_B and O_T–P–O_B angles.

the calculations but also those PO_4 units which are not threefold linked. The resulting angular distribution is shown in figure 3. The mean angle observed is 109°, which is typical of the tetrahedral geometry. The differentiation of the O_B–P–O_B and O_T–P–O_B angles results in means of 104 and 114°. These values are of the same magnitude as those known for the related P_2O_5 crystals [10, 12, 17]. The few angles larger than 145° belong to unreasonably distorted PO_4 units with O_B–O_B edges of about 0.3 nm, which are caused by the strain of some unsuitable network links.

The new distribution of P–O–P bridging angles also shown in figure 3 is narrowed and shifted to smaller angles if compared with that of the first RMC runs [2]. The mean of the bridging angles of the new RMC models is 139° instead of 141° as obtained before [2]. The decrease of the mean angle is due to the more realistic P–O_B distances of the new RMC models. In the new distribution a shoulder occurs at 160° whose origin is not clear. This questionable feature may cause the remaining differences with the angle of 137° which is calculated by the mean P–O_B and P–P distances [2]. Hence, we suggest a P–O–P bridging angle of 137° as being typical of the structure of v-P_2O_5. The real shape of the angular distribution is not fully constrained in the diffraction data because the P–P peak at 294 pm already interferes with P–O and O–O second-neighbour distances.

The use of larger Q-ranges of the neutron [1] and x-ray [16] data and the additional constraints improve the short-range order (SRO) of the models. What are the effects in the MRO? The P–P distances are the same as before [2], only the width of the peak is reduced. Thus, the distances between the centres of the PO_4 units are not changed. But the O_B–O_B edges are shortened from 253 to 249 pm, and the O_T–O_B edges are elongated from 253 to 258 pm. Since the P–P distances together with the O_B–O_B edges determine the extent to which the network of corner-linked PO_4 tetrahedra is stretched the decrease of the O_B–O_B lengths leads to a reorientation of network groups with more aligned O_B–O_B–O_B angles, i.e. the angles between the edges of two corner-linked PO_4 units. Actually, an increase of the

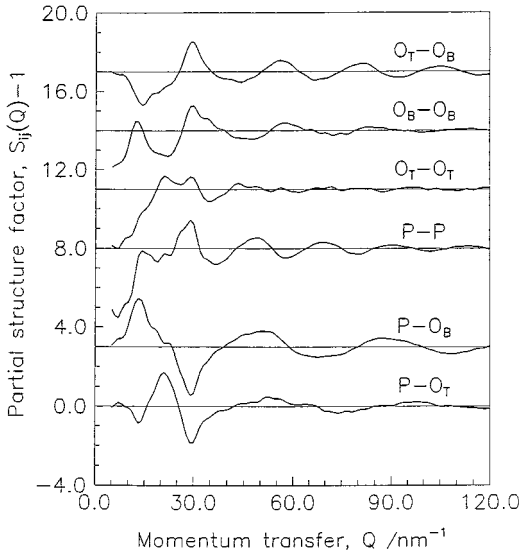

Figure 4. Partial structure factors, $S_{ij}(Q)$, of v-P_2O_5 averaged from six RMC models where the O_T and O_B sites are differentiated.

angles from 122.2 [2] to 125.6° (this work) is found. On the other hand, due to the increased O_T–O_B edges the unlinked apex of the tetrahedron becomes more distant from the networking O_B sites. Hence, more space is required to accommodate the O_Ts. These changes of the lengths of the tetrahedral edges should have subtle effects on the MRO of the new RMC models.

Information about the MRO is concentrated in the range of the first diffraction peaks. At first, the facts are repeated which we analysed in [2]. A remarkable feature of the $S_X(Q)$- [2, 9, 16] and also the $S_N(Q)$- [1, 11] data of v-P_2O_5 is the split first diffraction peak with two maxima (see figure 1) whose positions at 13 and 20 nm^{-1} were named Q_1 and Q_{1^*} [2]. The peak at Q_1 was interpreted [2] as the chemical order prepeak of a quasi-binary system of atoms and voids such as suggested for explanation of the first diffraction peak of amorphous Ge [14]. Due to the network links of a PO_4 unit only three P–P first neighbours exist while the number of P–P second neighbours is about 12, which was obtained from the corresponding peak in $g_{PP}(r)$ (cf figure 2). According to the atom-void model [14] the P–P second-neighbour distance of $R \cong 0.5$ nm is related to Q_1 by

$$Q \cong 7.7/R. \tag{2}$$

This is equivalent to $Q \cong 3\pi/2R$ [14] if the P–P first-neighbour distance of 294 pm is used. Equation (2) is known [14] as the relation between the position of a first diffraction peak of a disordered system of densely packed spheres and the first-neighbour distance. According to this equation a peak is also expected at 26 nm^{-1} for the first P–P distance of 294 pm which really exists in $S_{PP}(Q)$ (cf figure 4).

Considering the P and O species, contributions to the first peak at $Q_1 = 13$ nm^{-1} are found in all three partial structure factors $S_{PP}(Q)$, $S_{PO}(Q)$ and $S_{OO}(Q)$ [2]. The differentiation of the O_Ts and O_Bs results in six $S_{ij}(Q)$-functions, which are shown in figure 4. All partials which are not related to the O_T atoms have peaks at the position of the first diffraction peak. The $S_{POT}(Q)$ and $S_{OTOB}(Q)$ have minima at this position and $S_{OTOT}(Q)$ has no clear contribution. Thus, concerning the first peak the scattering of the P and O_B sites on one side and that of the O_T atoms on the other side are in antiphase. In order to illustrate the corresponding structural

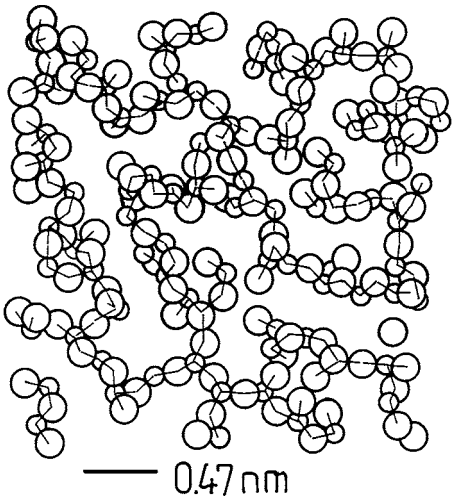

Figure 5. A slice of a RMC model of v-P_2O_5. Spheres of 0.14 and 0.18 nm in diameter illustrate the P and O_B sites, respectively. Thin lines are the P–O_B bonds. The thick line has a length of 0.47 nm and indicates the lateral dimension of the channel-like network cages. The O_Ts are not shown for clarity.

features slices of the model boxes are picked out where the O_T atoms are removed. An example of such slices is shown in figure 5 where the P and O_B sites are plotted as circles. The character of the slices is not much changed when they are selected from different configurations and when the directions of the boxes are varied. Numerous short channels surrounded by layer-like forms penetrate the slices. When instead of the O_Ts the P and O_B sites are neglected one would expect to see the same features where now the channels are highlighted. However, no clear MRO of the O_Ts is visible. This disorder in the packing of the O_T sites is also expressed in the lack of a clear contribution of the $S_{OTOT}(Q)$-function to the peak at Q_1. In the comparison with our first RMC work [2] an increase of the O_B–O_B–O_B angles was emphasized (cf above), which strengthens the order of the channel-like forms of P and O_B sites. Actually, in the older RMC models [2, 15] the channels were not visible so clearly as in the present models.

The lateral width, D, of the channels is equal to about 0.47 nm. If the first diffraction peak at Q_1 is interpreted as a quasi-Bragg peak with inter-layer distances equal to the channel width then, according to $Q = 2\pi/D$, Q_1 would be equal to 13 nm^{-1}, which is really observed. In some cases a few channels are stacked parallel. Three such layers are visible in figure 5 on the right-hand side. A repetition of more than two parallel layers seems to be not necessary to reproduce the peak at Q_1 and lattice-like regions are not observed on the whole.

The shoulder on the right-hand side of the first peak in $S_X(Q)$ or the second peak in $S_N(Q)$, both at Q_{1^*} of $\widetilde{=}$20 nm^{-1} (cf figure 1), are due to clear peaks in the $S_{POT}(Q)$- and $S_{OTOT}(Q)$-functions (cf figure 4). According to equation (2) a value R of $\widetilde{=}$0.35 nm would correspond to this peak. Such distances are really found in the P–O_T and O_T–O_T pair distributions of the RMC models (cf figure 2). Note that the $S_{POB}(Q)$-function has only a shoulder at this position. This shoulder is also known for the $S_{SiO}(Q)$-function of RMC models of v-SiO_2 [18], which is not visible in any of the total $S(Q)$-data.

4. Discussion

The features of the SRO in the new RMC models of v-P_2O_5 are more realistic than the older results [2]. The O–P–O angles within the tetrahedra show two maxima such as known for the threefold linked PO_4 units of the crystals [10, 12, 17]. But limits of the RMC approach of the structure of v-P_2O_5 become obvious with unreasonable spikes in some pair distances and a shoulder in the angular distribution of the P–O–P bridges. Similar to the RMC modelling of the structure of v-SiO_2 [18] two sets of scattering data are available for v-P_2O_5, i.e. the neutron [1] and x-ray [2] scattering data. But in v-P_2O_5 oxygen atoms with two different structural functions exist. In this work the O_T and O_B atoms were treated as different species but the different P–O and O–O first-neighbour peaks are only controlled by different coordination numbers and separation distances. Scattering makes no difference between the two O sites. There is no prospect of fully replacing the failing scattering information by other constraints. Nevertheless, valuable results on the MRO of v-P_2O_5 justify the application of the RMC approach.

At this stage we abandon further improvements of the models, which, finally, would amount to an introduction of interaction potentials. The RMC simulations are sensitive to geometric properties of the participating atoms. A small difference of the P–O_T and P–O_B distances was already found in our first RMC work [2], which is attributable to the steric effects of a different number of P neighbours. Another situation exists for the O–O tetrahedral edges. Here steric reasons are less effective to form short O_B–O_B and long O_T–O_B edges because the longer O_T–O_B edges belong to the triangles with the shorter P–O_T bonds [1, 10, 12, 17]. The different edge lengths are due to charge effects. An appropriate simulation exceeds the capabilities of RMC. The use of interaction potentials is required. The additional constraint of our RMC fit, i.e. the increased minimum separation of the O_T–O_B edges, acts as a repulsive force which results in the spikes obtained in the corresponding pair distributions.

The *ab initio* calculations from Uchino and Ogata [19] have not only reproduced the expected lengths of the P–O bonds but also the asymmetry of the PO_4 unit. The O_B–P–O_B and O_T–P–O_B angles obtained are 102 and 116°, respectively. The formal charges of the O_T and O_B sites, however, do not much vary. It is the large negative charge in the P–O_T bond overlap population, if compared with those in the P–O_B bonds, which causes the increase of the three O_T–P–O_B angles at the expense of the three O_B–P–O_B angles. The P–O–P angle in the bridge between the two simulated PO_4 units is 140° [19].

Other structural simulations of phosphate materials are made by the molecular dynamics (MD) method [20–24], among them also a first work [24] which includes v-P_2O_5. The interaction potentials used in [24] involve also terms of the O–P–O and P–O–P angles whose parameters are optimized to stabilize the three crystalline forms of P_2O_5. The MD results of v-P_2O_5 [24] reproduce the experimental bond lengths and bond angles [1, 2, 16]. The width of the distribution of O–P–O angles is comparable with our result but the width of the distribution of bridging angles obtained by MD is too narrow. At present, MD simulations of phosphate glasses [20–24] differ also from other experimental facts. The distributions of PO_4 groups (Q^n) with different numbers n of links are broader than experimentally observed [4, 25], e.g. only Q^3-units should exist in v-P_2O_5 but also significant fractions of Q^1, Q^2 and Q^4 are obtained by MD [24]. Also the P–O_B peaks of the MD models are too broad if compared with diffraction results [1, 26, 27]. These larger widths may result from the co-existence of the lots of unlike Q^n-units in the MD configurations. It is known [26, 27] that P–O_B distances bridging Q^n pairs of unlike n become more different, which increases the peak width of P–O_B distances. The undue links in the MD models may be attributable to the extremely high quenching rates of the glasses from the model melts, which is due to limitations of computer time. Ring size statistics

of the MD models are discussed [24], which we did not extract from our RMC models because of the network defects mentioned above.

The MD models of v-P_2O_5 [24] are too small to calculate model $S(Q)$-functions, and, thus, to study distances which are relevant for the first diffraction peaks. The MD configurations have only 54% of the P atoms in Q^3-units [24] while 82% of the P atoms of the RMC models are in Q^3-units. This fraction was 75% in our first RMC work [2]. The differences between RMC and MD are caused by a strict suppression of Q^4-units in our simulations. Therefore, a better formation of the specifics of a Q^3-network by RMC is expected. Since RMC also reproduces the first diffraction peaks the main features of the MRO of v-P_2O_5 should be developed in the models. According to the random process of RMC it produces less ordered structures than really exist. The formation of the channel-like structures with lateral widths of 0.47 nm results only from the constraints, i.e. from the $S(Q)$-data and the maximum coordination numbers used.

We remember the discussion of the MRO of v-As_2O_3 [28] whose networks, such as those of v-P_2O_5, are formed of threefold-linked units. Consequently, the numbers of AsO_3 (PO_4) units which form a connectivity polyhedron (or network cage) are larger than those of fourfold-linked SiO_4 units in v-SiO_2. This property of the Q^3-units reduces the stiffness of the network cages. Thus, the cages do not occupy their maximum space but they tend to flatten and Van der Waals forces hold together facing groups [28]. Here the layers are formed of the P and O_B atoms. The space between the layers is filled with the O_Ts, however, in a little ordered mode which becomes obvious when they instead of the O_Bs are shown in the slices of figure 5.

The distance which corresponds to the first diffraction peak is identified in discernible structures of the RMC models of v-P_2O_5 formed of the P and O_B atoms. If only the P sites are displayed, which, e.g., is shown in [15], then the formation of the channel-like structures is less conclusive. But one should also keep in mind that the increased O_B–O_B edges and decreased O_T–O_B edges such as quoted in section 3 change also the MRO if compared with that of our first RMC work [2]. The increased O_B–O_B–O_B angles indicate a flattening of the layer-like network areas and the accommodation of the O_Ts requires more space. The enhanced formation of the channel-like structures is due to the improvements of the SRO.

The structure of v-P_2O_5 bears more order than reflected by the simple scheme of atoms and voids [5, 14], where the discussion is reduced to pair distances such as made in our first analysis [2]. Moreover, not only layers of higher and lower atomic occupancy are formed such as reported for v-SiO_2 [6] but a visible layer-like network forms. The structure obtained by RMC can hardly be correlated with one of the P_2O_5 crystals [10, 12, 17]. Comparisons with the crystal structures were already made in [2]. The topology of stacked layers of form III [10] has a suitable inter-layer distance of 0.47 nm. But the density of this crystal is much too high. The P_2O_5 form II [17] has flat infinite channels but with highly ordered orientations of the P–O_T bonds. The P–P second-neighbour distances of the RMC models [2] match those found in form II [17] but not those of the forms I [12] and III [10].

5. Conclusions

The new reverse Monte Carlo analysis of the structure of vitreous P_2O_5 is improved to reproduce the anisotropy of the threefold-linked PO_4 network unit with different P–O_T and P–O_B bonds and different O_B–O_B and O_T–O_B edges. The resulting parameters of the short-range order are similar to those known for related crystals and those known from *ab initio* calculations of an $H_4P_2O_7$ cluster. The mean P–O–P bridging angle is 139 instead of 141° and the O_B–O_B–O_B angles in the links of PO_4 units are increased by 3° if compared with older RMC work. Both changes have subtle effects on the MRO. The formation of flattened network cages formed of

the P atoms and the O_B sites is intensified. The lateral dimension of the cages is 0.47 nm. This length is related to the first diffraction peak of the structure factors as a quasi-Bragg reflexion. This does not imply the existence of lattice-like regions. Finally, we reached the limits of RMC for modelling v-P_2O_5 because the differentiation of the O_B and O_T sites by different minimum separation distances leads to spurious spikes in some pair distributions.

Acknowledgments

Financial support of the Bundesministerium für Bildung und Forschung is gratefully acknowledged (grant 03-KR5ROK-9).

References

[1] Hoppe U, Walter G, Barz A, Stachel D and Hannon A C 1998 *J. Phys.: Condens. Matter* **10** 261
[2] Hoppe U, Walter G, Kranold R and Stachel D 1998 *Z. Naturf.* a **53** 93
[3] Galeener F L and Mikkelsen J C 1979 *Solid State Commun.* **30** 505
[4] Brow R K, Tallant D R, Hudgens J J, Martin S W and Irwin A D 1994 *J. Non-Cryst. Solids* **177** 221
[5] Elliott S R 1991 *Phys. Rev. Lett.* **67** 711
[6] Gaskell P H and Wallis D J 1996 *Phys. Rev. Lett.* **76** 66
[7] Wright A C, Hulme R A, Grimley D I, Sinclair R N, Martin S W, Price D L and Galeener F L 1991 *J. Non-Cryst. Solids* **129** 213
[8] Neuefeind J and Liss K-D 1996 *Ber. Bunsenges. Phys. Chem.* **100** 1341
[9] Walter G, Hoppe U, Kranold R and Stachel D 1994 *Phys. Chem. Glasses* **35** 245
[10] Stachel D, Svoboda I and Fuess H 1995 *Acta Crystallogr.* C **51** 1049
[11] Suzuya K, Price D L, Loong C-K and Martin S W 1998 *J. Non-Cryst. Solids* **232–234** 650
[12] Jansen M and Luer B 1986 *Z. Kristallogr.* **177** 149
[13] McGreevy R L and Pusztai L 1988 *Mol. Simul.* **1** 359
[14] Blétry J 1990 *Phil. Mag.* B **62** 469
[15] Hoppe U, Walter G, Kranold R, Barz A, Stachel D and Hannon A C 1998 *Glastechn. Ber. Glass Sci. Technol.* c **71** 192
[16] Hoppe U, Kranold R, Barz A, Stachel D and Neuefeind J 2000 *Solid State Commun.* **115** 559
[17] Arbib El H, Elouadi B, Chaminade J P and Darriet J 1996 *J. Solid State Chem.* **127** 350
[18] Wicks J D 1993 *PhD Thesis* Lincoln College, Oxford University
[19] Uchino T and Ogata Y 1995 *J. Non-Cryst. Solids* **181** 175
[20] Varshneya A K, Busbey R F and Soules T F 1985 *J. Non-Cryst. Solids* **69** 381
[21] Cormier G, Capobianco J A and Monteil A 1994 *J. Non-Cryst. Solids* **168** 115
[22] Boiko G G, Andreev N S and Parkachev A V 1998 *J. Non-Cryst. Solids* **238** 175
[23] Speghini A, Sourial E, Peres T, Pinna G, Bettinelli M and Capobianco J A 1999 *Phys. Chem. Chem. Phys.* **1** 173
[24] Liang J-J, Cygan R T and Alam T 2000 *J. Non-Cryst. Solids* **263–264** 167
[25] Hudgens J J, Brow R K, Tallant D R and Martin S W 1998 *J. Non-Cryst. Solids* **223** 21
[26] Hoppe U, Walter G, Stachel D, Barz A and Hannon A C 1997 *Z. Naturf.* a **52** 259
[27] Hoppe U, Kranold R, Stachel D, Barz A and Hannon A C 2000 *Z. Naturf.* a **55** 369
[28] Clare A G, Wright A C, Sinclair R N, Galeener F L and Geissberger A E 1989 *J. Non-Cryst. Solids* **111** 123